On the influence of build orientation on the mechanical properties of direct metal laser sintered (DMLS) Ti-6Al-4V flexures.

April 19, 2016

W.K. de Vree[1]

Abstract— **Flexures are beam shaped appliances that allow small displacements by bending the material, while constraining movement in other directions. The relative new techniques of additive manufacturing are becoming more mature and beneficial for businesses. One of the latest developments is Direct Metal Laser Sintering of titanium-alloy: Ti-6Al-4V, a material widely used in high-tech, high performance, medical, and flexure based applications.**
Mechanical properties of the material are studied on the level of research and development. In particular the influence of build orientation is investigated by means of testing samples printed at 0°, 45°and 90°. Results should indicate whether build orientation should be considered during design of flexure based products.
It was found that samples deviate in dimension from the design, mainly in the 90° and 45° build orientation. Partly due to layer orientation but also due to surface roughness which is found to be higher for the 90° and 45° build orientations. The surface roughness values found are 6.3 μm for 90°, 5.0 μm for 0° and 6.9 μm for 45°.
Ultimate tensile strength shows small differences in between build orientations: 1040 MPa for 90°, 1085 MPa for 0° and 1064 for 45°.
Also the fatigue limit estimations according to Dixon-Mood shows difference in between build orientations: 240 MPa for 90°, 285 MPa for 0° and 260 for 45°.
The results clearly show that build orientation should be accounted for when designing flexure based products for production with DMLS of Ti-6Al-4V.
Furthermore, a relation between the surface roughness, ultimate tensile strength and fatigue limit appears to exist for all build orientations.
Some inconsistency is found in the test results and further testing for reliability is recommended.

Nomenclature

- $Af[m^2]$: Measured cross section surface area of fatigue test sample
- $Af[m^2]$: Averaged measured cross section surface area of fatigue test sample
- $Af'[m^2]$: Designed cross section surface area of fatigue test sample
- AM : Additive Manufacturing
- $At[m^2]$: Measured cross section surface area of tensile test sample
- $At[m^2]$: Averaged measured cross section surface area of tensile test sample
- $At'[m^2]$: Designed cross section surface area of tensile test sample
- BD $[deg]$: Build Direction
- BO $[deg]$: Build Orientation
- DMLS : Direct Metal Laser Sintering
- K : Stress concentration factor
- $Kb[N/m]$: Bending stiffness
- R : Ratio between minimum and maximum stress of the stress cycles during a fatigue test
- $Ra[m]$: Surface roughness
- $S[Pa]$: Fatigue limit
- $S'[Pa]$: Fatigue limit based on designed geometry
- $S_{e,R_{90},C_{90}}[Pa]$: Fatigue limit with confidence level: 90% and reliability: 90%
- Ti-6Al-4V : Titanium alloy grade 5
- TS [Pa]: Tensile Strength
- UTS [Pa]: Ultimate Tensile Strength
- UTS' [Pa]: Ultimate Tensile Strength based on designed geometry
- σ : Standard deviation
- $\sigma_{bend}[Pa]$: bending stress
- $\sigma_{TS}[Pa]$: Tensile Strength
- $\sigma_{UTS}[Pa]$: Ultimate Tensile Strength

*This work is supported by TUDelft, Hittech Multin and 3T RPD

[1]W.K. de Vree is with Faculty of Mechanical Engineering, Technical University of Delft, The Netherlands W.K.deVree@student.tudelft.nl

I. INTRODUCTION

In high-tech sensitive precision equipment, flexures are often used to allow small displacements by bending the material. Flexures are simple, compact, light weight, relatively inexpensive and have very low friction. [1][2]
Due to high demands on the performance of flexures they are frequently made of the material titanium. Most often the alloy Ti-6Al-4V is concerned, which has desirable properties like high ductility, high strength, light weight, corrosion resistance and is commercially available. Another benefit of the material is it's bio compatibility for which it is highly desired in medical applications. However, the costs related to the material and the fabrication of wrought parts is always a concern [3]-[7].
Recent developments in 3D printing, or additive manufacturing (AM), allow for Ti-6Al-4V to be manufactured without loss of material and less labor. Further benefits of AM are it's design freedom and it has the prospect of faster and cheaper production for small batches. AM uses a computer model of the product and prints it layer-by-layer, with the layers perpendicular to the build direction (BD). In almost all cases the layers are horizontal as the BD is vertical. The method of Direct Metal Laser Sintering (DMLS) uses a laser to sinter layers of powdered material and create a solid structure [8][9]. However, the structure of the end material is different from conventional produced parts, which are machined from a solid cast of the material [3].
Surface roughness is a measure of the topographic relief of a surface and is known to influence other mechanical properties.
Ultimate tensile strength (UTS) is a measure often used by engineers to define the strength of a material and is the value of static stress at which a material fails.
Metal fatigue is one of the main causes of failure in cyclically loaded elements like flexures. The failure is due to the repetition of a load applied below the yield strength of the material. The fatigue limit is the stress, expressed in MPa, below which the material will not fail, even when cyclically loaded. Factors known to influence the fatigue strength of a material are the microstructure, surface conditions, stress concentrations, load type i.a. [10][11][12].

The overall goal of this research is to determine the mechanical properties of stress relieved DMLS Ti-6Al-4V on the level of research and development. This can be used to decide whether this production method is applicable for flexure based designs.
Of particular interest in this research is the influence of the build orientation (BO) during AM on the surface roughness, UTS and fatigue limit of the flexure. The BO is defined by the orientation of the long axis of the flexure relative to the horizontal. It is of essence whether the BO should be taken into account during design of flexure based products.
Furthermore, a relation between UTS, surface roughness and the fatigue limit of a material is found to exist and is also handled in this research. [10]

Studies have been performed to specify the mechanical properties of the AM Ti-6Al-4V. Mainly the microstructure, tensile strength, surface conditions and influence of heat treatments and other postprocessing [13]-[26]. However, the influence of BO is moderately studied and none is found on the mechanical properties of DMLS Ti-6Al-4V [27].
For usability of the novel Ti-6Al-4V DMLS technique it is of great importance for engineers and designers to know all mechanic and dynamic relations of the resulting material and whether BO should be accounted for. In this work the relation between the BO and the surface roughness, UTS and fatigue limit of DMLS Ti-6Al-4V is attempted to determine through experiments and analysis of results and possible relations will be determined.

II. EXPERIMENTAL PROCEDURE

To determine the relation between BO and mechanical properties of DMLS Ti-6Al-4V, the surface roughness, UTS and fatigue limit will be determined for various BO. For these tests several test samples are prepared and the first research is on the manufacturing process and samples them self.

A. DMLS

All test samples are DMLS Ti-6Al-4V, produced by 3T RPD, built on an EOS M280 using standard EOS Ti64 parameters [9]. The Ti-6Al-4V powder is added in layers of $\pm 60\mu m$ with a particle size of $15-45\mu m$. The powder is sintered with a 200 Watt fibre laser. The build chamber atmosphere is Argon and its temperature is room temperature. After the AM procedure, all samples are annealed in one batch by computer controlled heating at 800° C for four hours.

TABLE I
PRODUCTION PARAMETERS

System	EOS M280
Power source	200 W fibre laser
Powder particle-size	$15-45\mu m$
Layer-thickness	$60\mu m$
Chamber atmosphere	Argon
Chamber temperature	Room temperature
Annealing process	at 800° C for 4 Hrs.

In this research the BO's 0°, 45° and 90° will be considered, where the 90° BO is vertical and parallel to the build direction (BD), the 0° is horizontal, and 45° is at an angle of 45° with respect to both horizontal and vertical as depicted in Fig. 1.

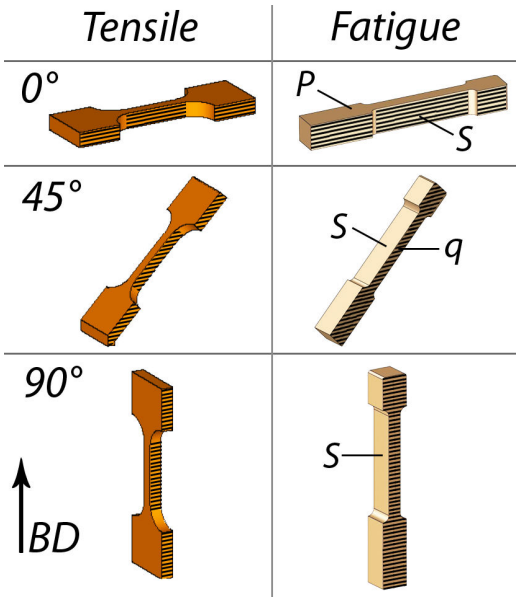

Fig. 1. BO's, with BD vertical

The surfaces indicated by *S* are the surfaces of interest for the surface roughness research, as at these surfaces the fatigue cracks are expected to nucleate. Photo's of these surfaces at 4x magnification are shown in Fig. 2 to Fig. 4. The surface indicated by *p* in Fig. 1 is the 'top' surface where the path of the laser will be visible and a photo of this surface is shown in Fig. 5. The surface indicated by *q* shows the 'side' surface of the 45° build, which shows layers in 45° and a photo of this surface is shown in Fig. 6.

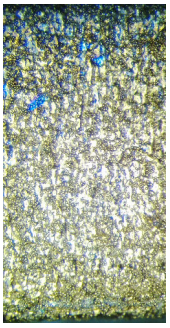

Fig. 2. S, 90°

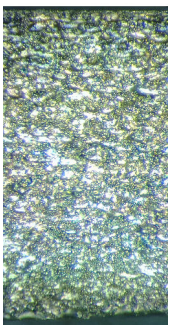

Fig. 3. S, 0°

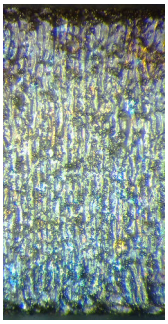

Fig. 4. S, 45°

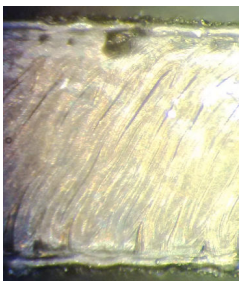

Fig. 5. p, 0°

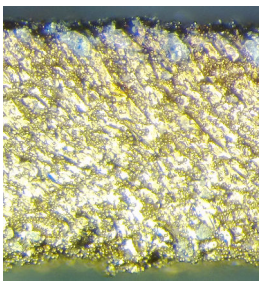

Fig. 6. q, 45°

Non of the samples show defects and/or abnormalities apart from traces of mechanically removing material. After building all samples need to be removed from a base. Only the 45° samples need support printed, which is removed after manufacturing. The removing of support and/or base leaves various sections of the builds with a smooth surface. This is not expected to influence the strength of the sample as this smooth area is not near the area of failure from tensile and fatigue test.

B. Surface roughness

Surface roughness is measured by the *Ra* value in μm which is the mean of absolute measured values. The value is calculated by equation 1 [38].

$$Ra = \frac{1}{n}\sum_{i=1}^{n}|y_i| \tag{1}$$

Where n indicates ordered, equally spaced points along a trace over the surface, and y_i is the vertical distance from the mean line to the i^{th} data point. The optical microscope Bruker K1 is used to scan all 18 fatigue test samples. The scan area is at the center of the surface *S* as indicated in Fig. 1 where the fatigue crack is expected to nucleate. The scan area is of size 1.15 mm by 0.23 mm. The *Ra* value is measured from the scans, after removal of waviness, at 10 places with the Bruker K1 software. The average *Ra* value will be presented per BO.

C. Tensile tests

Per BO three tensile tests are performed for a total of nine tests. The test machine used is the Instron 5500R and the method and test samples according to NEN-EN-ISO 6892. The dimensions of the samples are depicted in Fig. 7. The test is performed at standard conditions.

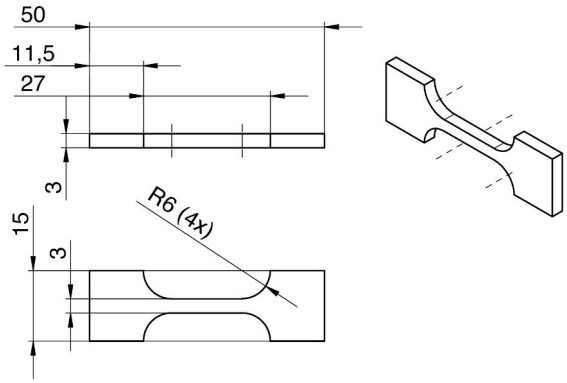

Fig. 7. Tensile test sample dimensions

Prior to testing, the smallest cross sections: At, of the tensile test samples are measured with a caliper on three different locations per sample. The cross section measurement averages per orientation: At_{avg}, designed cross sections: At' and the deviation from the designed cross section are tabulated in table II.

TABLE II
MEASURED AND DESIGNED CROSS SECTIONS OF THE TENSILE TEST SAMPLES

Orientation	$At_{avg}[mm^2]$	At' $[mm^2]$	Dev. [%]
90°	9.64	9	7.1
0°	9.61	9	6.7
45°	10.11	9	12.3

The Instron 5500R measures the force during the tests and the tensile strength (TS) is calculated as:

$$\sigma_{TS} = \frac{F[N]}{A[m^2]}[Pa] \tag{2}$$

Where F is the force and A the surface area of the cross section perpendicular to the force. The UTS is the highest measured tensile strength during the test. The UTS will be calculated for the measured and designed cross sections.

D. Bending Fatigue tests

Per BO six fatigue tests are performed for a total of 18 tests. The test machine is the Instron ElectroPuls^{TM} E10000, with a one kN load cell. To perform the two point bending test a setup was specially designed and mounted [28]. A model of the setup is shown in Fig. 8, where A is a double hinged bar which transmits the reciprocating force. The bar is clamped at the tip of the flexure which is indicated by D. The other end of the flexure is clamped by clamp C which is mounted to the base B. A photo of the setup is shown in Fig. 9.

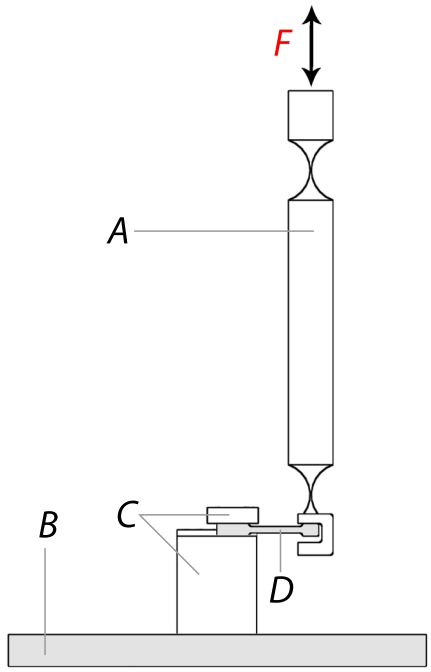

Fig. 8. Model of the specially designed test setup.

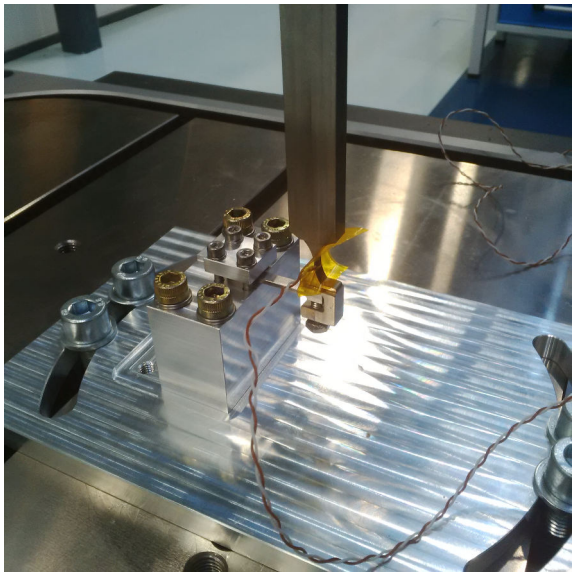

Fig. 9. Close up of test setup with flexure mounted

The resulting stress in the designed flexure due to an applied force is analyzed using Finite Element Analysis [28] with an accuracy of 1%. This relation has shown very linear behavior as deviations are small and is shown in appendix. More details of the test setup and FEA are found

in the design report [28].

Via the staircase method [10] a sequence of tests is performed according to NEN-ISO 12107. A load is applied sinusoidal with constant amplitude and maximum stress starting with an estimate of the fatigue limit of the samples; 230 MPa for the 90° and 45° and 250 MPa for the 0° build orientation [27]. Depending on the survival or failure of the previous test sample, the next sample will be tested at a higher or lower load with an interval d of 10 MPa. The tests are performed at 20 Hz, with R = -1, at standard conditions. The R ratio indicates in this case a fully reversed test and is calculated as:

$$R = \frac{\sigma_{[min]}[Pa]}{\sigma_{[max]}[Pa]} \tag{3}$$

Failure is detected by an increase in deviation of 10%. The test is stopped when a sample fails or at 10^6 cycles.
The dimensions of the samples are depicted in figure 10, and have a stress concentration factor K of 1.2 according to Peterson's [29].

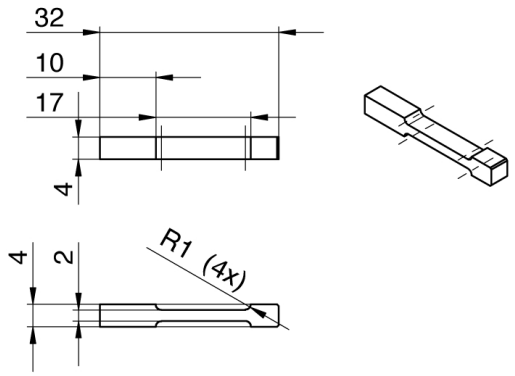

Fig. 10. Fatigue test sample dimensions

Prior to testing, the smallest cross sections Af, of the fatigue test samples are measured with a caliper on three different locations per sample. The cross section measurement averages per orientation Af_{avg}, designed cross sections: Af' and the deviation from the designed cross section are tabulated in table III.

TABLE III
MEASURED AND DESIGNED CROSS SECTIONS OF THE FATIGUE TEST SAMPLES

Orientation	$Af_{avg}[mm^2]$	$Af'[mm^2]$	Dev. [%]
90°	9.14	8	14.3
0°	9.18	8	14.8
45°	9.89	8	23.6

The staircase test results will be presented and the data will be analyzed according to Dixon-Mood [10]. The data will also be converted to the measured dimensions.

E. Mechanical relations

A fatigue limit prediction method provides us with relations between the surface roughness (Ra), UTS and fatigue limit [10]. The fatigue limit estimate S_e can be estimated by modifying the bending fatigue limit (S_{be}) with the four factors: loading type (C_L), surface finish (C_S), size (C_D) and reliability level (C_R) as shown in equation 4.

$$S_e = S_{be} \cdot C_L \cdot C_S \cdot C_D \cdot C_R \cdot \frac{1}{K_f} \tag{4}$$

For bending fatigue limit (S_{be}) at 10^6 cycles for wrought steels can be estimated as 0.5 times the UTS for materials with UTS $<$ 1400 MPa. Variable C_S depends on the Ra value and the UTS and its value can be derived from a graph with empirically based data. K_f is the stress concentration factor adopted for bending fatigue.
Loading type C_L and size factor C_D are equal for all samples with a value of 1. The reliability level will be ignored reducing the equation to:

$$S_e = S_{be} \cdot C_S \cdot \frac{1}{K_f} \tag{5}$$

For the calculation method of C_S and K_f the author refers to the design report [28].

III. HYPOTHESIS

In general it was found from research that the 0° BO of AM metals has a higher UTS and fatigue limit then the 45° and 90° BO. The 45° and 90° BO are almost about the same value [19][20][22]. The UTS has higher values (factor 0.25 - 0.6) than the fatigue limit and also larger deviation then the fatigue limit data. The surface roughness, UTS and fatigue limit are empirically related. In general a higher UTS means a higher fatigue limit. The opposite is found to be true for the surface roughness (Ra), the higher the surface roughness the lower the fatigue limit [10].
It is assumed this relation still holds for DMLS Ti-6Al-4V. However, the method is based on conventional fatigue limit predictions (not for AM) and researches on AM metals. Therefor no BO is considered in the prediction model and the applicability of research results on other AM metals is doubtful [27][30].
Fig 1 shows the orientation of the layers for the different BO's. This shows the layers being directed in the length of the sample and this way it can bear most load. Also the 0° BO exists of less but larger layers. On the contrary for the 45° and 90° BO, which show that all connections

between layers need to bear load and is expected to be weaker than the 0° BO [19][20][22][8].
As after heat treatment, microstructure was found not to be influenced by BO (macrostructure) this is ignored in this research [25].

The expected values of the UTS and fatigue limit follow from literature research [27] and are tabled in table IV.

TABLE IV
ESTIMATED UTS AND FATIGUE LIMITS S

BO	UTS [MPa]	S [MPa]
90°	1050	200
0°	1100	220
45°	1050	200

Considering surface roughness a staircase effect arises when building occurs under an angle.

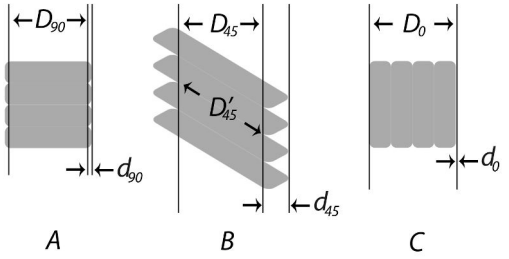

Fig. 11. Illustration of layer orientation and surface effects.

Due to this effect it is expected that the 45° shows the highest Ra value followed by 90° BO and 0° BO with the lowest value. From research it is also found that the 0° BO has a smoother surface than any surface built under an angle since the laser beam melts that surface directly. Other variables known to influence the surface roughness are the scan speed of the laser during DMLS and the laser power. Only a rough estimate of the *Ra* value are possible to derive from comparable researches on AM metals and relative material as no *Ra* data is available of the exact material [25][31][32][33].
The estimate values are shown in the table below.

TABLE V
ESTIMATED Ra_{est} VALUES PER BO

BO	$Ra_{est}[\mu m]$
90°	4-11
0°	4-10
45°	4-14

IV. RESULTS

A. Surface roughness

Fig. 12 - 14 show surface scans of the surface S as indicted in Fig. 1.

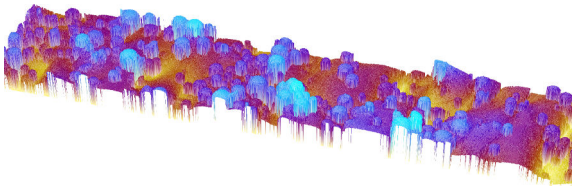

Fig. 12. Scan of typical surface S, 90° BO

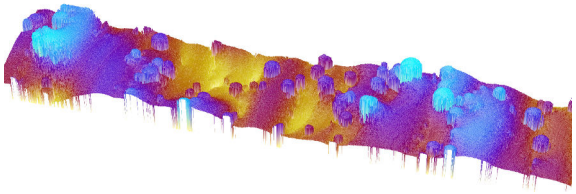

Fig. 13. Scan of typical surface S, 0° BO

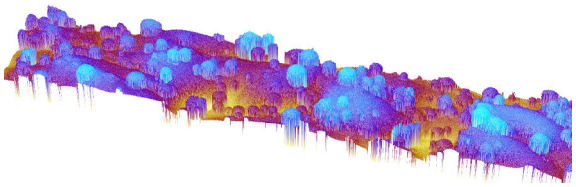

Fig. 14. Scan of typical surface S, 45° BO

Table VI shows the averages of the measured *Ra* values of the surfaces S, per orientation including standard deviations.

TABLE VI
AVERAGED RA VALUES PER BO WITH STANDARD DEVIATIONS

BO	$Ra_{avg}[\mu m]$	σ
90°	6.3065	0.9164
0°	4.9830	1.5148
45°	6.9108	1.3331

B. Tensile tests

The results of all nine tests are presented in Fig. 15 and 16. In Fig. 15, the cross section is taken as the measured cross section of the concerning sample: At. In Fig. 16 the cross section is taken as the designed cross section: At' as presented in table II.

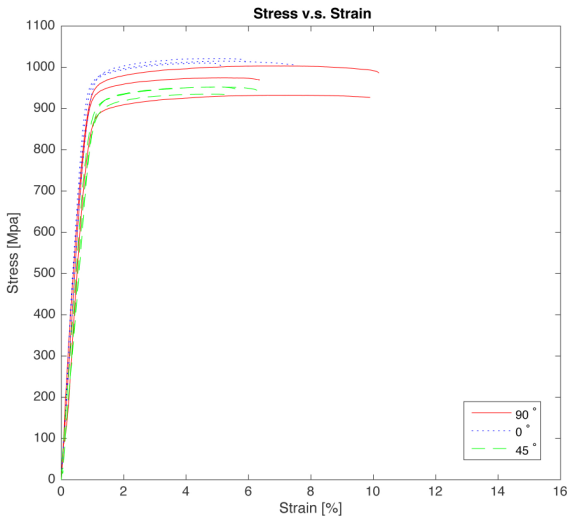

Fig. 15. Tensile test results with cross section At (as measured)

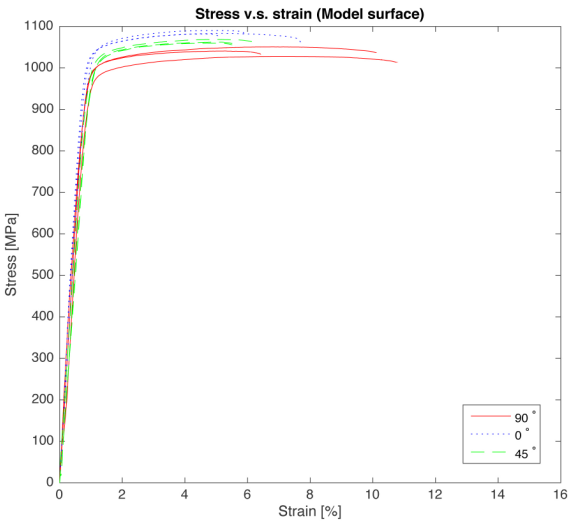

Fig. 16. Tensile test results with cross section At' (as designed)

The average UTS are presented, with the same division in cross sections, together with the standard deviations: σ, in table VII.

TABLE VII
UTS AVERAGE FOR A AND A' WITH STANDARD DEVIATIONS

BO	$\sigma_{UTS}(At)$ [MPa]	σ	$\sigma_{UTS}(At')$ [MPa]	σ
90°	970	36	1040	11
0°	1015	6	1085	4
45°	946	10	1064	5

C. Bending Fatigue tests

Prior to testing, the bending stiffness Kb of the sample is determined. The averages per BO and standard deviation are shown in table VIII.

TABLE VIII
AVERAGED BENDING STIFFNESS PER ORIENTATION

BO	Kb_{avg} [N/mm]	σ
90°	127	2
0°	126	5
45°	123	5

Finite Element Analysis was performed on the flexure model (with designed dimensions) to determine the maximum stress in the flexure at a particular load. First the fatigue limit results based on the designed dimensions (S') are presented.
The staircase test results are shown in Fig. 17. A circle indicates a sample that did not fail prior to 10^6 cycles. A cross or star indicates a sample failure during the test. The amount of cycles at which the sample failed is stated in the legend.

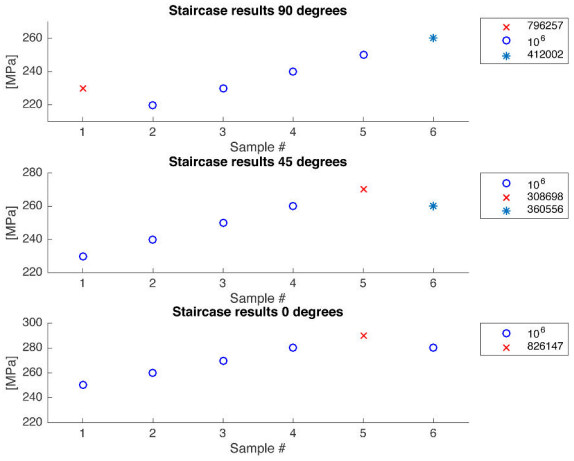

Fig. 17. Staircase test results for all BO's

According to Dixon-Mood the $S_{e,R_{90},C_{90}}$ value is the fatigue limit with confidence level: 90% and reliability: 90%.

Maximum likelihood estimates of the fatigue limits together with the standard deviation according to Dixon-Mood [10], assuming normal distribution and the the $S_{e,R_{90},C_{90}}$ value are shown in table IX.

TABLE IX
FATIGUE LIMITS PER BO ACCORDING TO DIXON-MOOD [10]

BO	$S'[MPa]$	σ	$S_{e,R_{90},C_{90}}$
90°	240	37	148
0°	285	5	272
45°	260	5	247

Adapted with Svensson-Loren [34], which states that for small sample sizes the standard deviation should be multiplied by a factor two.

TABLE X

FATIGUE LIMITS PER BO ACCORDING TO DIXON-MOOD [10] ADAPTED WITH SVENSSON-LOREN

BO	$S'[MPa]$	σ	$S_{e,R_{90},C_{90}}$
90°	240	74	56
0°	285	11	259
45°	260	11	234

The stress occurring in the flexure can be adapted to the measured dimensions. Formula 6 provides the relation between the maximum bending stress σ_{bend} in the flexure and it's dimensions.

$$\sigma_{bend} = \frac{Fbh^2}{6L}[Pa] \tag{6}$$

Where F is the applied force at the tip of the flexure, b the width, h the height and L the length of the flexure. With constant F and L, higher b and h result in higher stress. Table XI shows the percentages by which the measured b and h exceed the designed b and h. The factor $\frac{b \cdot h^2}{b' \cdot h'^2}$ provides an estimate by which the maximum stress in the flexure should be multiplied to adapt for the measured dimensions.

TABLE XI

PERCENTILE DIMENSIONS EXCEEDANCE OF FATIGUE TEST SAMPLES ON AVERAGE AND MULTIPLICATION FACTOR

BO	$b[\%]$	$h[\%]$	$\frac{b \cdot h^2}{b' \cdot h'^2}$
90°	4.0	9.9	1.26
0°	3.5	11.0	1.28
45°	3.9	19.2	1.47

Approximate of the stress occurring in the flexures with measured dimensions are given in table XII.

TABLE XII

FATIGUE LIMIT RESULTS FROM DESIGNED DIMENSIONS AND ADAPTED FATIGUE LIMIT TO MEASURED DIMENSIONS

BO	$S'[MPa]$	$S[MPa]$
90°	240	301
0°	285	363
45°	260	382

D. Mechanical relations

The estimated value of the fatigue limit S_e are tabled in table XIII. As the estimate is based on the UTS, estimates using the UTS data from both designed (S'_e) and measured (S_e) cross section are presented.

TABLE XIII

ESTIMATED FATIGUE LIMITS AND FACTORS OF S AND S' FROM FATIGUE TEST RESULTS RELATIVE TO ESTIMATED FATIGUE LIMITS

BO	$S'_e[MPa]$	$\frac{S'}{S'_e}$	$\frac{S}{S'_e}$	$S_e[MPa]$	$\frac{S'}{S_e}$	$\frac{S}{S_e}$
90°	316	0.76	0.95	296	0.81	102
0°	334	0.85	1.09	313	0.91	116
45°	310	0.84	1.23	276	0.94	138

Below the results of comparing fatigue limit to UTS and surface roughness (Ra) are shown. The difference between the values of the different BO's are of interest.

TABLE XIV

RATIO'S OF FATIGUE LIMITS TO UTS AND Ra

BO	$\frac{S'}{UTS'}$	$\frac{S'}{UTS}$	$\frac{S'}{Ra}$	$\frac{S}{UTS'}$	$\frac{S}{UTS}$	$\frac{S}{Ra}$
90°	0.231	0.247	38.1	0.289	0.310	47.8
0°	0.263	0.254	57.0	0.335	0.358	72.6
45°	0.244	0.275	37.7	0.359	0.404	55.4

V. DISCUSSION

In order to determine the influence of build orientation on the mechanical properties of DMLS Ti-6Al-4V a series of tests were performed and results are presented. In this section the procedure of tests and analysis of the results is discussed.

The tested material is assumed to have a density of near 100% and is practically non-porous. Prior to testing, the surface of all samples were checked on defects/abnormalities but non were found. Consequently, early crack initiation and/or failure due to defects, cavities and porosity were not considered.
Furthermore, residual stresses are considered to be non existing as the samples are heat treated [13][35].
Microstructural influence is researched elsewhere and is found not to influence the relation between build orientation (macrostructure) and the mechanical properties significantly (after heat treatment) and therefore not included in this research [25]. However, it is recommended to study the microstructure of the sample material and determine whether the assumptions made above are valid.

A. DMLS samples

Examination of the samples has shown quite great difference in geometry between the design and the manufactured parts. The 90° and 0° builds show larger geometry due to surface conditions as specified by the manufacturer to be about $15\mu m$. The 45° build shows more deviation from the designed geometry in all samples as was hypothesized due to the layer orientation resulting

in larger protuberance at the surface.

Referring to Fig. 11, the 'core' of the sample should have the dimensions as specified by the designer to withstand the stresses during life time as indicated in by D. The area indicated by d in Fig. 11 does not contribute to bearing the load. For that reason, results from both measured dimensions and designed dimensions are presented and one could consider either one of the results, depending on the design situation. Note that the effect should diminish with decreasing layer thickness.

B. Surface roughness

Looking at the surfaces of the samples in Fig. 2 to Fig. 4 the 90° and 45° BO show visibly rougher surface relative to the 0° BO. This corresponds to the explanation of higher geometry of the samples as shown on figure 11. But not only the layer structure contributes to this as the surface scans in Fig 2 to Fig. 3 show rougher surface for the 90° and 45° BO mainly due to unmelted Ti-6Al-4V powder grains. These two factors result in the higher Ra values for the 90° and 45° BO then the 0° BO as shown in table VII.
However, these grains do not induce early crack initiation (influence on fatigue) and also do not contribute in bearing any load. On the contrary it is found from research that the unmelted grains do induce stress concentrations. [25]

Further investigation of the surface conditions of the test samples could shed light on the dilemma of the effective load bearing cross section including Rv (valley depth) and waviness.

C. Tensile strength

The stress-strain curves shown in Fig. 15 and Fig. 16 show nice linear behavior (modulus of elasticity) until yield strength. This is a good indication of properly produced samples without defects and abnormalities.

For analyzing the tensile strength a division was made between the designed dimensions and measured dimensions for reasons mentioned in section V-A of this discussion. The difference between the results of measured and designed cross section is explained by the relation of the tensile strength and the cross section of the sample as shown by equation 2.

The test results indicate in both situations that the 0° build has the highest UTS as expected. A second factor contributing are the unmelted powder grains which are far more apparent in the 90° and 45° BO then in the 0° BO which can induce stress concentrations as mentioned in the previous section.

The tensile strength of the 45° build becomes lower when calculated with the measured cross section. This is because the measured cross section is larger while the outer layer of this larger cross section is not likely to sustain much load. The extra material d might bear a little load due to round offs and/or coincidental connections between the layers at the surface but not as much as section D. The effect is also apparent with the 90° BO, but less than at the 45° BO which shows a large difference in strength between the two situations.
The structure of the 45° BO makes the surfaces between the layers larger and more surface for the layers to weld together as indicated by D' in Fig. 11. On the down side this also gives more possibility for pores and stress concentrations. So it is highly debatable whether the measured cross sections D and d i.c.w. possible stress concentrations and BO make for a stronger or weaker construction. And thus it is also not possible to determine whether the differences in strength between the BO is due to layer orientation, or merely due to the deviation in dimensions and surface conditions resulting from the BO.

Looking at the standard deviations of both situations, the results calculated for the designed surface show much lower standard deviation. This is often an indication that these results are more reliable [37].
The results also comply with the expectation of the tensile strength of the material. Especially in the case calculated with the designed dimensions.

During tensile testing prior to the failure the sample deforms and begins to neck. The actual cross section of the sample effectively bearing the load reduces and the true UTS is actually higher than the calculated UTS in this research [39][40][41]. Due to the already complicated measurement of the cross section this is passed in this research. If desired the fractured cross sections can be measured and the true stress can be calculated.

D. Fatigue limit

The bending stiffness of all three orientations are very alike and consistent (low standard deviation). This is again an indication that the test samples are without defects and abnormalities.

When analyzing the fatigue data, again the division was made between the designed and

measured dimensions. The dimensions of the fatigue samples deviate about the same amount from the design but due to the smaller cross section than the tensile test samples the deviation is a larger percentage of the original dimensions as shown in table III. Again the 45° BO has largest dimensions and deviates most from the design.
In this case the fatigue limit for the measured dimensions is calculated via equation 6 from the maximum stress occurring according to the finite element analysis (FEA). The equation however is only an indication of the maximum bending stress in a material. Furthermore, the results are very peculiar as the measured width d and especially height h deviate quite a bit from the design. As was discussed in the previous section it is very unlikely that the maximum stress actually occurs in the samples as the section d does not bear as much load as D from Fig. 11. Especially because formula 6 uses h^2 while the outermost part of the cross section is just a spread of unmelted grains which can be up to 45 μm. Meaning that the calculated maximum stress actually never occurs during the bending fatigue test.
Also, fatigue crack growth is known to initiate at a crack or notch if it exists at the surface [10]. Meaning that the crack will start at a point within the surface and not at the outermost point and thus at a lower stress than is calculated using the measured dimensions.
Lastly, the results recalculated for measured dimension do not comply with the expectations for both the absolute values and the differences between orientations.
Therefor in the rest of this discussion the results from the designed geometry are considered.

It was observed that the fatigue limit estimate via Dixon-Mood of samples built at 0° has the highest value of 285 MPa, followed by 45° with a value of 260 MPa and lowest is the 90° BO with a value of 240 MPa.
Striking is the first fatigue failure during the test for the 90° BO. The sample failed at a relative low stress of 230 MPa and the second failure only occurred at 260 MPa. This is an indication for inconsistency in the samples fatigue limits and results in a relative low fatigue limit estimate and large standard deviation. When analyzing for reliability the fatigue limit becomes even lower due to the large standard deviation and after applying Svensson-Loren theory for small sample sizes, gives a fatigue limit estimate with confidence level: 90% and reliability: 90% of only 56 MPa.
In this research it was assumed that samples would have near 100% density and no porosity and/or defects, while these factors influence fatigue life greatly [10][25]. The results of the 90° BO indicates that builds are not as consistent, dens and without defects as assumed and that samples should be inspected carefully prior to use or should be post processed. Also the high surface roughness and geometry deviation was unexpected. These factors indicate that early crack initiation due to surface conditions might not be ignored and it is again recommended to further investigate this.

During the fatigue tests for the 0° BO only one sample failed. This result does not give any insight in the consistency of the fatigue failure of the 0° BO, even though the standard deviation according to Dixon-Mood is only 5 MPa.
The 45° test result shows two adjacent failures. This is a desired situation as it shows consistency in the data and small standard deviation.
However, note that the Dixon-Mood data analysis does not account for the amount of cycles to failure. Looking at the amount of cycles to failure of the 45° BO the values are strikingly low. This might again be an indication of inconsistent material properties between samples.
Considering the above it is recommend to analyze all samples thoroughly and perform more fatigue tests for reliability.
Also inspecting the fracture surface of the samples might give insight on whether a crack has nucleated or a crack already existed at the surface and whether porosity is indeed negligible.

E. Mechanical relations

The estimated fatigue limits according to [10] are calculated in [28]. The estimated values are higher than the hypothesized values. This is not surprising as the estimation method is based on wrought steel which has a superior microstructure than AM Ti-6Al-4V [13] [14]. However, the relations between the BO's do comply with the expectation that 0° BO has the highest fatigue limit, followed by 90° and last the 45° BO.

Looking at the ratio's of the resulted fatigue limit from tests to the estimated fatigue limit in table XIII, a higher consistency is visible when considering the fatigue limit from designed dimensions (S'). The $\frac{S'}{S'_e}$ shows factors with only a difference of 0.08 and the $\frac{S'}{S_e}$a difference of 0.13. In contrast the ratios calculated with the fatigue limits from measured dimensions are 0.28 and 0.36 apart. Considering that the results from the fatigue tests are expected to comply with the estimation method it might be argued that the results from designed dimensions are most realistic.

Looking at the ratio's in table XIV only $\frac{S'}{UTS}$, $\frac{S'}{UTS'}$ and $\frac{S'}{Ra}$ show some consistency as the values of the different BO are close together relative to the values calculated with measured dimensions. Next to that they comply to the expectations that 0° has the highest UTS and fatigue limit. For $\frac{S'}{UTS}$ it complies even more to the expectation that the 45° has the lowest UTS and fatigue limit.

VI. CONCLUSION

The goal of this research was to determine some mechanical properties of stress relieved DMLS Ti-6Al-4V without other post processing, on the level of research and development. Eventually to determine the applicability of the material in flexure based products. The influence of build orientation on mechanical properties was investigated by surface scanning the sample surface and tests on tensile strength and fatigue strength of samples built at 0°, 45°, and 90°. The results should indicate whether build orientation should be taken into account during the design process.

The samples have shown large deviation in dimensions form design and high surface roughness. Here a distinction can already be made between the BO's as the measured dimensions exceed the designed dimensions more for the 90° and 45° BO than the 0° BO. The difference in dimensions can be addressed to the layer structure difference between BO's but also unmelted grains at the surface which are more apparent at the for the 90° and 45° BO than the 0° BO.
The surface roughness is found to be higher for the for the 90° and 45° BO than the 0° BO as expected and is presented in table VI.
It is recommended to further investigate the surface properties of the material including waviness and the impact of the surface conditions on the effective cross section and stress concentrations.

The real UTS is found difficult to determine due to the large deviations in dimension and surface roughness. This is due to the fact that tensile strength is calculated by force over cross section and the effective cross section of the sample is hard to determine. Therefor results are considered for both designed and measured as presented in table VII. However, expectations, standard deviation and relations between *Ra*, UTS and fatigue limit indicate that the results calculated with designed dimensions are more realistic and presented in table VII in the right column.
It is recommended to perform more tensile tests for reliability. Possibly controlling for surface roughness and cross sectional area to exclude the encountered difficulties when the influence of BO on UTS is investigated further.

Also for determining the fatigue limit the effective cross section complicates the matter. The resulting maximum stress in the flexure was analyzed using finite element analysis on the model with designed dimensions. Again the expectations, standard deviation and relations between *Ra*, UTS and fatigue limit indicate that the results calculated with designed dimensions are more realistic. Moreover, because fatigue cracks are more likely to start at an existing crack or notch. Thus the results presented in table IX are assumed most realistic and the results presented in X most reliable.
Considering the fatigue limit data from designed dimensions as shown in table IX the results are higher than expected from literature research. This indicates a superior material than was found in researches on which the estimations were based.
Noteworthy is the lower value and large standard deviation of the 90° BO which is an indication of inconstancy in the material. The single failure during staircase testing the 0° BO and cycles to failure are other indications for inconsistency for all BO's.
It is highly recommended to perform more fatigue tests for all BO's for reliability. Again possibly controlling for surface roughness and cross sectional area to exclude the encountered difficulties when the influence of BO on UTS is investigated further.

A relation between surface roughness, UTS and fatigue limit appears to still exist in heat treated DMLS Ti-6Al-4V as the factors similarity shown in table XIV considering 'designed' indicate.

The test results are a good indication of mechanical properties of heat treated DMLS Ti-6Al-4V. It should be noted that all results are on the level of research and development. The results show that BO should be taken into account when designing flexure based products. Furthermore, the results show indications of inconsistency in material properties in between samples so overall it is highly recommended to perform more test for reliability.

REFERENCES

[1] Koster, M.P., "Constructieprincipes", pp 114, 1996.
[2] Lobontiu, N., "Complient Mechanisms", *Design of flexure hinges*,P 58, 2003.
[3] Donachie, M.J., "Titanium: a technical guide", 2000.
[4] Materials Properties Handbook: Titanium Alloys, R. Boyer, G. Welsch, and E. W. Collings, eds. ASM International, Materials Park, OH, 1994.
[5] Metals Handbook, Vol.2 - Properties and Selection: Nonferrous Alloys and Special-Purpose Materials, ASM International 10th Ed. 1990.

[6] Metals Handbook, Vol. 3, Properties and Selection: Stainless Steels, Tool Materials and Special-Purpose Metals, Ninth Edition, ASM Handbook Committee., American Society for Metals, Materials Park, OH, 1980.

[7] Structural Alloys Handbook, 1996 edition, John M. (Tim) Holt, Technical Ed; C. Y. Ho, Ed., CINDAS/Purdue University, West Lafayette, IN, 1996.

[8] McGee, W., de Leon M.P., "Robotic Fabrication in Architecture, Art and Design", 2014

[9] http://www.3trpd.co.uk/dmls.htm, "Metal Additive Manufacturing (AM) using Direct Metal Laser Sintering (DMLS)", 2014.

[10] Lee, Y., Pan, J., Hathaway, R., Barkey, M., "Fatigue testing and analysis", 2005.

[11] Weibull, W., "Fatigue testing and analysis of results", 1961.

[12] Forrest, P.G., "Fatigue of Metals", 1970.

[13] S. Leuders, M. Thone, A. Riemer, T. Niendorf, T. Troster, H.A. Richard, H.J. Maier, *On the mechanical behaviour of titanium alloy TiAl6V4 manufactured by selective laser melting: Fatigue resistance and crack growth performance*, 2012.

[14] Suo Hongbo, Chen Zheyuan, Liu Jianrong, Gong Shuili, Xiao Jianzhong, *Microstructure and Mechanical Properties of Ti-6Al-4V by Electron Beam Rapid Manufacturing*, 2014.

[15] M. Simonelli, Y.Y. Tse, C. Tuck, *Effect of the build orientation on the mechanical properties and fracture modes of SLM Ti–6Al–4V*, 2014.

[16] Bernd Baufelda, Erhard Brandl, Omer van der Biest, *Wire based additive layer manufacturing: Comparison of microstructure and mechanical properties of Ti–6Al–4V components fabricated by laser-beam deposition and shaped metal deposition*, 2011.

[17] Bernd Baufeld, Omer Van der Biest, Rosemary Gault, *Additive manufacturing of Ti–6Al–4V components by shaped metal deposition: Microstructure and mechanical properties*, 2009.

[18] P. Edwards, M. Ramulu, *Fatigue performance evaluation of selective laser melted Ti–6Al–4V*, 2014.

[19] H. Khalid Rafi, Thomas L. Starr, Brent E. Stucker, *A comparison of the tensile, fatigue, and fracture behavior of Ti–6Al–4V and 15-5 PH stainless steel parts made by selective laser melting*, 2013.

[20] Kai Guan, Zemin Wang, Ming Gao, Xiangyou Li, Xiaoyan Zeng, *Effects of processing parameters on tensile properties of selective laser melted 304 stainless steel*, 2013.

[21] Todd M. Mower, Michael J. Long, *Mechanical behavior of additive manufactured, powder-bed laser-fused materials*, 2015.

[22] Suraj Rawal, James Brantley, Nafiz Karabudak *Additive Manufacturing of Ti-6AI-4V Alloy Components for Spacecraft Applications*, 2013.

[23] Erhard Brandla, Christoph Leyens, Frank Palma, *Mechanical properties of additive manufactured Ti-6Al-4V using wire and powder based processes*, 2009.

[24] Idan Rosenthal, Adin Stern, Nachum Frage, *Microstructure and Mechanical Properties of AlSi10Mg Parts Produced by the Laser Beam Additive Manufacturing (AM) Technology*, 2014.

[25] Erhard Brandl a, Ulrike Heckenberger, Vitus Holzinger, Damien Buchbinder, *Additive manufactured AlSi10Mg samples using Selective Laser Melting (SLM): Microstructure, high cycle fatigue, and fracture behavior*, 2011.

[26] Monika Blattmeier, Gerd Witt, Johannes Wortberg, Jan Eggert, Jochen Toepker, *Influence of surface characteristics on fatigue behaviour of laser sintered plastics*,Rapid Prototyping Journal, Vol. 18 Iss 2 pp. 161 - 171, 2012.

[27] De Vree, W.K., *Estimation of fatigue limit of DMLS Ti-6Al-4V in varying build orientations*, 2016.

[28] De Vree, W.K., *Design fatigue test setup*, 2016.

[29] Pilkey, W. D., "Peterson's Stress Concentration Factors", 1997.

[30] De Vree, W.K., *Preliminary research; Fatigue testing of 3D printed titanium flexures*, 2016.

[31] J. Delgado, J. Ciurana, C.A. Rodríguez "Influence of process parameters on part quality and mechanical properties for DMLS and SLM with iron-based materials", 2011.

[32] F. Calignano, D. Manfredi, E. P. Ambrosio, L. Iuliano, P. Fino, "Influence of process parameters on surface roughness of aluminum parts produced by DMLS", 2012.

[33] A.B. Spierings, T.L. Starr, K. Wegener, "Fatigue performance of additive metallic parts", 2000.

[34] R. Pollak, A. Palazotto, T. Nicholas, "A simulation-based investigation of the staircase method for fatigue strength testing", 2006.

[35] Callister, W.D., "Fundamentals of materials science and engineering", *Chapter 11.10, "Heat treatments"*, second edition, 2005.

[36] Vernon, J., "Testing of materials," *Chapter 6, Fatigue and Fatigue Testing*, pp. 69-77, 1992.

[37] van Beek, A., "Advanced engineering design", 2009.

[38] Degarmo, E.P., Black J., Kohser R.A., "Materials and Processes in Manufacturing" (9th ed.), 2003

[39] A. C. Mackenzie, J. W. Hancock, and D. K. Brown, "On the influence of state of stress on ductile failure initiation in high strength steels," Engineering Fracture Mechanics, vol. 9, no. 1, pp. 167–188, 1977.

[40] E. E. Cabezas and D. J. Celentano, "Experimental and numerical analysis of the tensile test using sheet specimens," Finite Elements in Analysis and Design, vol. 40, no. 5-6, pp. 555–575, 2004.

[41] K. T. Jaquess and K. Frank, "Characterization of the Material Properties of Rolled Sections," Tech. Rep. SAC/BD-99/07, SAC Joint Venture, USA, 1999.